Published for SISSA by Springer

Received: *May 2, 2019*
Accepted: *July 23, 2019*
Published: *August 5, 2019*

Three-dimensional finite temperature Z_2 gauge theory with tensor network scheme

Yoshinobu Kuramashi and Yusuke Yoshimura

Center for Computational Sciences, University of Tsukuba,
1-1-1, Tennodai, Tsukuba, Ibaraki, Japan

E-mail: kuramasi@het.ph.tsukuba.ac.jp, yoshimur@ccs.tsukuba.ac.jp

Abstract: We apply a tensor network scheme to finite temperature Z_2 gauge theory in 2+1 dimensions. Finite size scaling analysis with the spatial extension up to $N_\sigma = 4096$ at the temporal extension of $N_\tau = 2, 3, 5$ allows us to determine the transition temperature and the critical exponent ν at high level of precision, which shows the consistency with the Svetitsky-Yaffe conjecture.

Keywords: Duality in Gauge Field Theories, Lattice QCD

ArXiv ePrint: 1808.08025

https://doi.org/10.1007/JHEP08(2019)023

Contents

JHEP08(2019)023

1 Introduction

Tensor network algorithms for coarse-graining of the classical partition functions were originally developed in the field of condensed matter physics [1–4]. In 2007 the tensor renormalization group (TRG) was proposed by Levin and Nave to study two-dimensional (2D) classical models [3]. This work attracted the attention of elementary particle physicists so that exploratory studies were performed for 2D scalar models consisting of continuous variables [5] with the TRG method. To study wider variety of models in elementary particle physics with the tensor network algorithms, however, it is necessary to develop efficient algorithms for fermion systems and gauge theories. Recently one of the authors and his collaborator have successfully applied the Grassmann tensor renormalization group (GTRG) [6–8] to determine the phase diagram of the one-flavor Schwinger model with and without the θ term employing the Wilson fermion formulation [6, 9, 10], which are the first applications of the GTRG method to lattice gauge theory including fermions in the path integral formalism. The analyses of these models explicitly demonstrated that the GTRG method does not suffer from the sign problem and the complex action problem. Furthermore, direct treatment of the Grassmann numbers in the GTRG method provides us another virtue that the computational cost is comparable to the bosonic case. This work was followed by an investigation of one-flavor 2D Gross-Neveu model with finite chemical potential [11] and 2D $\mathcal{N} = 1$ Wess-Zumino model [12]. The GTRG method was also applied to 3D fermionic systems [13, 14]. On the other hand, it has been difficult to develop an efficient tensor network algorithm for gauge theories because of its redundancy of gauge degrees of freedom. Although a couple of attempts have been made so far [15–18], the question of their efficiency for lattice gauge theories still remains.

In this paper we apply the tensor network scheme to a study of 3D finite temperature Z_2 gauge theory on the $V = N_\sigma^2 \times N_\tau$ lattice. This is a good test bed for the first feasibility

study of tensor network scheme for lattice gauge theories. Especially the finite temperature phase transition of this model was already investigated in detail by the high-precision Monte Carlo calculation with the aid of the duality to the 3D Ising spin model [19]. Numerical efficiency of our method is demonstrated by investigating the phase transition with the use of finite size scaling analyses, in which the spatial extension N_σ is varied up to 4096 at $N_\tau = 2, 3, 5$. It is another virtue of the tensor network scheme that the computational cost is in proportion to the logarithm of the system size so that we can take very large volume regarded as the thermodynamic limit. The results for the transition temperature and the critical exponent ν are compared to those obtained by the Monte Carlo method [19]. We also discuss the consistency with the Svetitsky-Yaffe conjecture [20].

This paper is organized as follows. In section 2 we explain a tensor network scheme and associated numerical algorithm to treat the 3D Z_2 gauge theory. Numerical results for the finite temperature phase transition of 3D Z_2 gauge theory is presented in section 3. Section 4 is devoted to summary and outlook.

2 Tensor network scheme

2.1 Tensor network formulation

The partition function of three-dimensional Z_2 gauge theory is given by

$$Z = 2^{-3V} \sum_{\{\sigma=\pm1\}} \prod_{n,\mu>\nu} e^{-\beta\sigma_{n,\mu\nu}} \tag{2.1}$$

with

$$\sigma_{n,\mu\nu} = \sigma_{n,\mu}\sigma_{n+\hat{\mu},\nu}\sigma_{n+\hat{\nu},\mu}\sigma_{n,\nu}, \tag{2.2}$$

where $\sigma_{n,\mu} \in \{-1, 1\}$ is defined on the link labeled by a site $n = (n_0, n_1, n_2)$ with a direction $\mu = 0, 1, 2$. $\hat{\mu}$ and $\hat{\nu}$ denote unit vectors in μ and ν directions, respectively.

We first construct the tensor network representation of eq. (2.1) following ref. [15]. Each Boltzmann factor at site n is expanded by

$$\begin{aligned} e^{\beta\sigma_{n,\mu\nu}} &= \cosh\beta \sum_{p=0,1} (\tanh\beta)^p \sigma_{n,\mu\nu}^p \\ &= \cosh\beta \sum_{p_{n,\mu,\nu},q_{n,\nu,\mu},q_{n,\mu,\nu},p_{n,\nu,\mu}=0,1} B^{(n,\mu\nu)}_{p_{n,\mu,\nu}q_{n,\nu,\mu}q_{n,\mu,\nu}p_{n,\nu,\mu}} \sigma_{n,\mu}^{p_{n,\mu,\nu}} \sigma_{n+\hat{\mu},\nu}^{q_{n,\nu,\mu}} \sigma_{n+\hat{\nu},\mu}^{q_{n,\mu,\nu}} \sigma_{n,\nu}^{p_{n,\nu,\mu}}, \end{aligned} \tag{2.3}$$

where we introduce the tensor B by

$$B_{pqrs} = (\tanh\beta)^{(p+q+r+s)/4} \delta_{p,q}\delta_{q,r}\delta_{r,s}. \tag{2.4}$$

We can collect the terms involving a $\sigma_{n,\mu}$ and sum over it. For example, the case of $\sigma_{n,0}$ is expressed as

$$\sum_{\{\sigma_{n,0}=\pm1\}} \sigma_{n,0}^{p_{n,0,1}+p_{n,0,2}+q_{n-\hat{1},0,1}+q_{n-\hat{2},0,2}} = 2A^{(n,\mu=0)}_{p_{n,0,1}p_{n,0,2}q_{n-\hat{1},0,1}q_{n-\hat{2},0,2}}, \tag{2.5}$$

JHEP08(2019)023

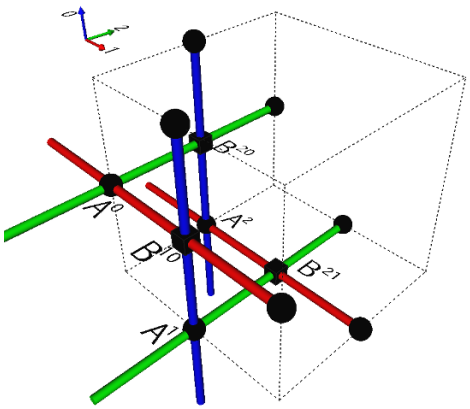

Figure 1. Tensor network for Eq . (2.7). Dotted lines describe the cubic lattice. Black cubes and spheres represent B and A, respectively. Red, blue and green bars denote the contractions of the tensor indices.

where

$$A_{pqrs} = \delta_{\text{ mod }(p+q+r+s,2)=0}. \tag{2.6}$$

So the partition function can be rewritten as the following tensor network representation:

$$Z = (\cosh\beta)^{3V} \sum_{\{p,q\}} \prod_{n,\mu>\nu} B^{(n,\mu\nu)} \prod_{n,\mu} A^{(n,\mu)}. \tag{2.7}$$

The connections between tensors are depicted in figure 1.

In addition, we reconstruct the tensor network representation to reduce the redundant degrees of freedom. Taking $\mu = 0$ as the temporal direction and $\mu = 1, 2$ as the spatial ones, we classify the sites as spatially even sites l with

$$\text{mod }(l_1 + l_2, 2) = 0 \tag{2.8}$$

and spatially odd sites m with

$$\text{mod }(m_1 + m_2, 2) = 1. \tag{2.9}$$

Let us rearrange the tensors so that all the tensors are collected at the spatially even sites. In this procedure, we employ the gauge fixing with $\sigma_{m,0} = 1$ at the spatially odd sites $m(m_0 \neq 0)$. Then, all the components of $A^{(m,0)}$ are one constantly and so we can omit the $A^{(m,0)}$ i.e. sum up independently the indecies $p_{m,0,1}, p_{m,0,2}, q_{m-\hat{1},0,1}$ and $q_{m-\hat{2},0,2}$. At the $m_0 = 0$ sites, $A^{(m,0)}$ are decomposed as

$$A^{(m,0)}_{p_{m,0,1}p_{m,0,2}q_{m-\hat{1},0,1}q_{m-\hat{2},0,2}} = \sum_{i=0,1} \bar{A}^{(m-\hat{1})}_{q_{m-\hat{1},0,1}p_{m,0,2}i} \bar{A}^{(m-\hat{2})}_{q_{m-\hat{2},0,2}p_{m,0,1}i}, \tag{2.10}$$

$$\bar{A}_{pqi} = \delta_{\text{ mod }(p+q+i,2)=0} \tag{2.11}$$

JHEP08(2019)023

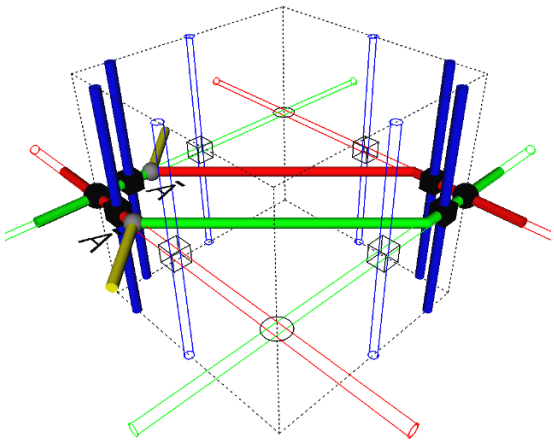

Figure 2. Decomposition of $A^{(m,0)}$ at the $m_0 = 0$ sites. Gray spheres represent $\bar{A}$.

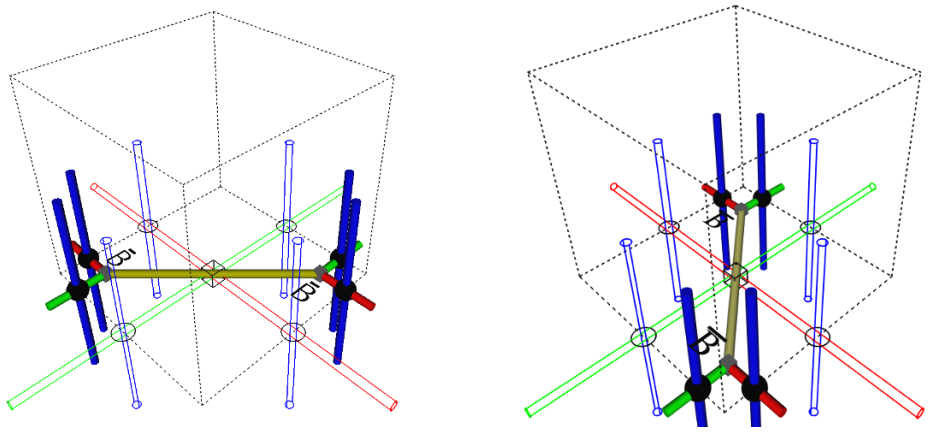

Figure 3. Decomposition of $B^{(l,21)}$ (left) and $B^{(m,21)}$ (right). Gray cubes represent $\bar{B}$.

as illustrated in figure 2. On the other hand, $B^{(n,21)}$ are decomposed as

$$B^{(l,21)}_{p_{l,2,1}q_{l,1,2}q_{l,2,1}p_{l,1,2}} = \sum_{i=0,1} \bar{B}^{(l)}_{p_{l,1,2}p_{l,2,1}i} \bar{B}^{(l+\hat{1}+\hat{2})}_{q_{l,1,2}q_{l,2,1}i}, \tag{2.12}$$

$$B^{(m,21)}_{p_{m,2,1}q_{m,1,2}q_{m,2,1}p_{m,1,2}} = \sum_{i=0,1} \bar{B}^{(m+\hat{2})}_{p_{m,2,1}q_{m,1,2}i} \bar{B}^{(m+\hat{1})}_{q_{m,2,1}p_{m,1,2}i}, \tag{2.13}$$

$$\bar{B}_{pqi} = (\tanh\beta)^{(p+q)/4} \delta_{p,q} \delta_{q,i} \tag{2.14}$$

as illustrated in figure 3. After contracting all the inner indices of the collected tensors, we

JHEP08(2019)023

obtain new tensors T on the sites of $l_0 > 0$ as

$$
\begin{aligned}
T^{(l)}_{xyzx'y'z'} = & \sum_{p,q} A^{(l,0)}_{p_{l,0,1}p_{l,0,2}q_{l-\hat{1},0,1}q_{l-\hat{2},0,2}} \\
& \cdot B^{(l,10)}_{p_{l,1,0}q_{l,0,1}z_1p_{l,0,1}} B^{(l,20)}_{p_{l,2,0}q_{l,0,2}z_2p_{l,0,2}} B^{(l-\hat{1},10)}_{p_{l-\hat{1},1,0}q_{l-\hat{1},0,1}z_3p_{l-\hat{1},0,1}} B^{(l-\hat{2},20)}_{p_{l-\hat{2},2,0}q_{l-\hat{2},0,2}z_4p_{l-\hat{2},2,0}} \\
& \cdot A^{(l,1)}_{p_{l,1,2}p_{l,1,0}q_{l-\hat{2},1,2}z'_1} A^{(l,2)}_{p_{l,2,0}p_{l,2,1}z'_2q_{l-\hat{1},2,1}} A^{(l-\hat{1},1)}_{p_{l-\hat{1},1,2}p_{l-\hat{1},1,0}q_{l-\hat{1}-\hat{2},1,2}z'_3} A^{(l-\hat{2},2)}_{p_{l-\hat{2},2,0}p_{l-\hat{2},2,1}z'_4q_{l-\hat{2}-\hat{1},2,1}} \\
& \cdot \bar{B}^{(l)}_{p_{l,1,2}p_{l,2,1}x} \bar{B}^{(l)}_{q_{l-\hat{1},2,1}p_{l-\hat{1},1,2}y} \bar{B}^{(l)}_{q_{l-\hat{1}-\hat{2},1,2}q_{l-\hat{1}-\hat{2},2,1}x'} \bar{B}^{(l)}_{p_{l-\hat{2},2,1}q_{l-\hat{2},1,2}y'}
\end{aligned} \tag{2.15}
$$

and S on the sites of $l_0 = 0$ as

$$
\begin{aligned}
S^{(l)}_{xyzx'y'z'} = & \sum_{p,q} A^{(l,0)}_{p_{l,0,1}p_{l,0,2}q_{l-\hat{1},0,1}q_{l-\hat{2},0,2}} \bar{A}^{(l)}_{q_{l,0,1}x_2y'_2} \bar{A}^{(l)}_{q_{l,0,2}x_3y_2} \\
& \cdot B^{(l,10)}_{p_{l,1,0}q_{l,0,1}z_1p_{l,0,1}} B^{(l,20)}_{p_{l,2,0}q_{l,0,2}z_2p_{l,0,2}} B^{(l-\hat{1},10)}_{p_{l-\hat{1},1,0}q_{l-\hat{1},0,1}z_3x'_3} B^{(l-\hat{2},20)}_{p_{l-\hat{2},2,0}q_{l-\hat{2},0,2}z_4x'_2} \\
& \cdot A^{(l,1)}_{p_{l,1,2}p_{l,1,0}q_{l-\hat{2},1,2}z'_1} A^{(l,2)}_{p_{l,2,0}p_{l,2,1}z'_2q_{l-\hat{1},2,1}} A^{(l-\hat{1},1)}_{p_{l-\hat{1},1,2}p_{l-\hat{1},1,0}q_{l-\hat{1}-\hat{2},1,2}z'_3} A^{(l-\hat{2},2)}_{p_{l-\hat{2},2,0}p_{l-\hat{2},2,1}z'_4q_{l-\hat{2}-\hat{1},2,1}} \\
& \cdot \bar{B}^{(l)}_{p_{l,1,2}p_{l,2,1}x_1} \bar{B}^{(l)}_{q_{l-\hat{1},2,1}p_{l-\hat{1},1,2}y_1} \bar{B}^{(l)}_{q_{l-\hat{1}-\hat{2},1,2}q_{l-\hat{1}-\hat{2},2,1}x'_1} \bar{B}^{(l)}_{p_{l-\hat{2},2,1}q_{l-\hat{2},1,2}y'_1}
\end{aligned} \tag{2.16}
$$

as illustrated in figure 4. Redefining the spatial even sites l as the new sites n, we obtain the final form of the tensor network representation:

$$
Z = \sum_{\{t,x,y\}} \left(\prod_{n;n_0>0} T^{(n)} \right) \left(\prod_{n;n_0=0} S^{(n)} \right), \tag{2.17}
$$

where t (x, y) denotes the temporal (spatial) indices in the new network. Note that the spatial size of the new network is half of the original one.

2.2 Algorithm for coarse graining

Our algorithm consists of three steps. Firstly we repeat coarse-graining of the tensor T in the temporal direction using the HOTRG method [21] until the temporal size of T is reduced to be one. In figure 5 we illustrate the procedure for the case of $N_\tau = 5$. The dimension of the new tensors T' and T'' is set to be $D_1 = 16$, with which the HOTRG calculation is exact up to two iterations of the coarse-graining procedure.

Secondly we apply the HOTRG procedure to the combination of T and S making the trace of their temporal indices as depicted in figure 6. The dimension of the new tensor S' is kept to be $D_1 = 16$. After this procedure we are left with the two-dimensional tensor network system.

Thirdly we make coarse-graining of the two-dimensional system until the size is reduced to be 2×2 where the contraction of the indices are exactly carried out. In this work we employ the TRG method for coarse-graining with D_2 as the truncation parameter of the tensor dimensions.[1]

[1] We need to increase D_1 and D_2 if we take much larger N_τ.

JHEP08(2019)023

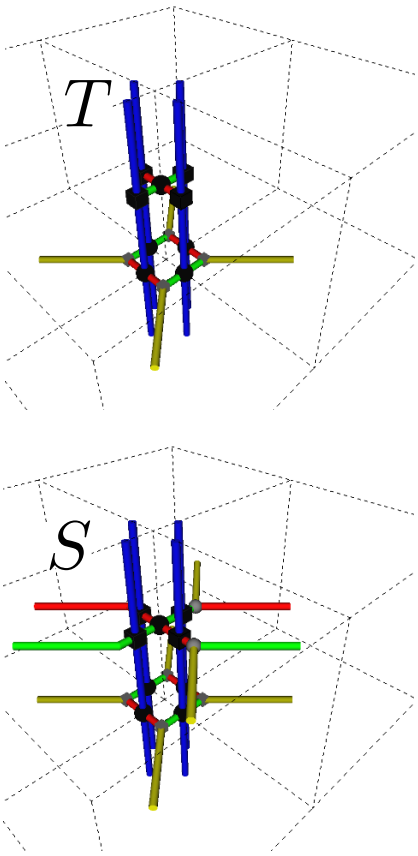

Figure 4. Tensors T (top) and S (bottom) in eq. (2.17).

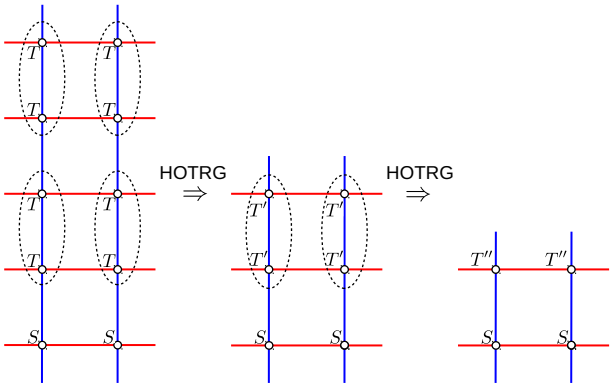

Figure 5. The first step of the algorithm. Blue (red) line denotes the temporal (spatial) direction. After two iterations of the HOTRG procedure, the temporal size of the tensor T is reduced to be one.

JHEP08(2019)023

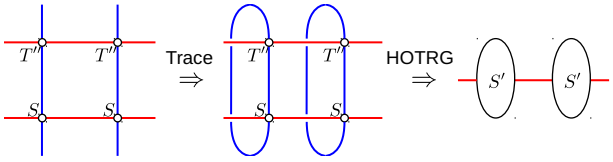

Figure 6. The second step of the algorithm. Blue (red) line denotes the temporal (spatial) direction.

3 Numerical study

3.1 Setup

We determine the phase transition temperature β_c and the critical exponent ν applying the finite size scaling analyses to the specific heat:

$$C(N_\sigma) \equiv \beta^2 \frac{\partial^2 \ln Z}{V \partial \beta^2}. \tag{3.1}$$

The values of β_c and ν are compared with the previous high-precision Monte Carlo results [19].

Numerical study of 3D Z_2 gauge theory is performed by employing the algorithm explained in section 2 on the $N_\sigma^2 \times N_\tau$ lattice with the periodic boundary condition. We fix the temporal extension at $N_\tau = 2, 3, 5$. The spatial lattice size is varied up to $N_\sigma = 4096$ in order to make finite size scaling analyses toward the thermodynamic limit. In figure 7 we plot the D_2 dependence of $(\ln Z)/V$ and $\delta_F = |1 - \ln Z(D_2)/\ln Z(D_2 = 160)|$ at $\beta = 0.71115$ on the $4096^2 \times 3$ lattice, which illustrate a convergence behavior of $(\ln Z)/V$ almost on the phase transition point as a representative case. We observe that the value of $(\ln Z)/V$ monotonically converges as D_2 increases. Since we find similar behaviors at other β values, we take the results with $D_2 = 128$ as the central values and their errors are estimated by the difference from those with $D_2 = 144$.

3.2 Results

In figure 8 we plot the specific heat of eq. (3.1) as a function of $1/\beta$. We observe the clear peak structure at all the values of N_σ and the peak height $C_{\max}(N_\sigma)$ grows as N_σ increases. In order to determine the peak position $\beta_c(N_\sigma)$ and the peak height $C_{\max}(N_\sigma)$ at each N_σ we employ the quadratic approximation of the specific heat around $\beta_c(N_\sigma)$:

$$C(N_\sigma) \sim C_{\max}(N_\sigma) + R\left(\frac{1}{\beta} - \frac{1}{\beta_c(N_\sigma)}\right)^2$$

with R a constant. Instead of fitting the specific heat itself we fit the internal energy E with the following form around $\beta_c(N_\sigma)$:

$$E = -\frac{\partial \ln Z}{V \partial \beta} = P + \frac{C_{\max}(N_\sigma)}{\beta} + \frac{R}{3}\left(\frac{1}{\beta} - \frac{1}{\beta_c(N_\sigma)}\right)^3$$

with P another constant. This procedure suffers from less uncertainties associated with the numerical derivative compared to the direct fit of the specific heat itself.

JHEP08(2019)023

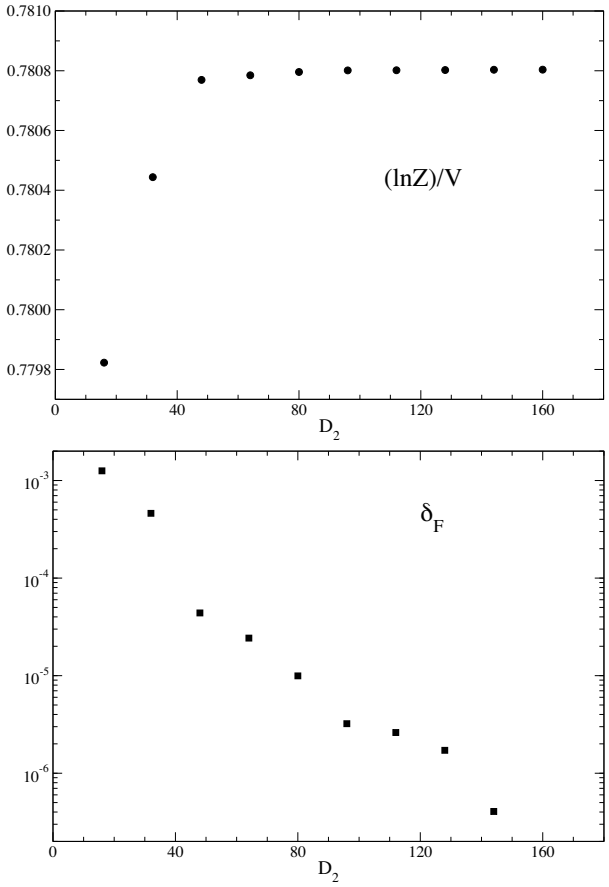

Figure 7. D_2 dependence of $(\ln Z)/V$ (top) and δ_F (bottom) at $\beta = 0.71115$ on the $4096^2 \times 3$ lattice.

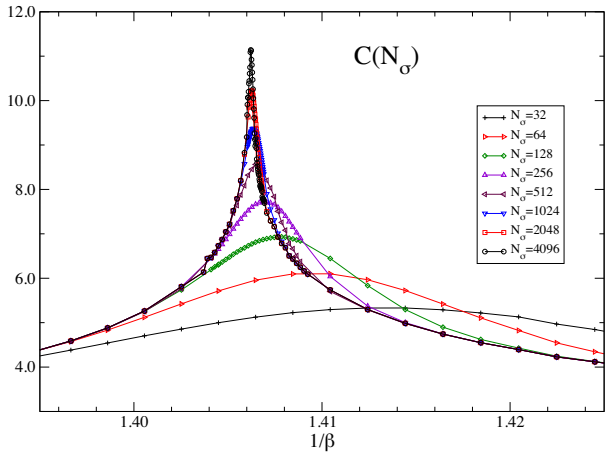

Figure 8. Specific heat $C(N_\sigma)$ at $N_\tau = 3$ as a function of $1/\beta$ with $N_\sigma \in [32, 4096]$.

JHEP08(2019)023

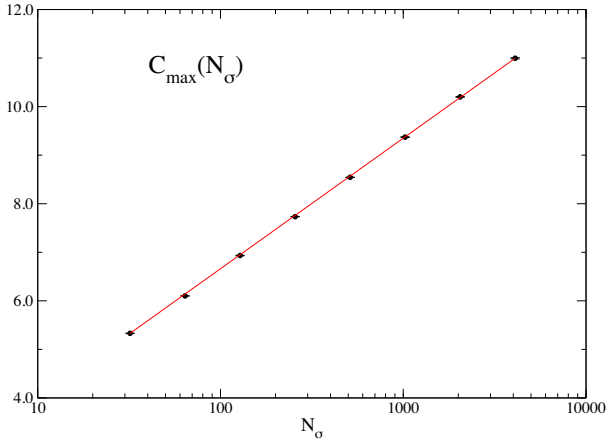

Figure 9. Peak height of specific heat $C_{\max}(N_\sigma)$ at $N_\tau = 3$ as a function of N_σ. The horizontal axis is logarithmic. Solid line is to guide your eyes.

We expect that the peak height $C_{\max}(N_\sigma)$ scales with N_σ as

$$C_{\max}(N_\sigma) \propto N_\sigma^{\alpha/\nu}, \tag{3.2}$$

with the critical exponents α and ν. We plot the peak height $C_{\max}(N_\sigma)$ at $N_\tau = 3$ as a function of N_σ in figure 9. We observe a clear logarithmic N_σ dependence for $C_{\max}(N_\sigma)$. We have found similar features at other N_τ. These observation indicates $\alpha \simeq 0$. We can determine another critical exponent ν from the finite size scaling behavior of the peak position $\beta_c(N_\sigma)$,

$$\beta_c(N_\sigma) - \beta_c(\infty) \propto N_\sigma^{-1/\nu}. \tag{3.3}$$

Figure 10 shows N_σ dependence of $\beta_c(N_\sigma)$ at $N_\tau = 3$ as a representative case. The solid curve represents the fit result obtained with the fit function of $\beta_c(N_\sigma) = \beta_c(\infty) + BN_\sigma^{-1/\nu}$. In table 1 we list the fit range at each N_τ which is chosen to avoid possible finite size effects due to the smaller N_σ. The fit results for $\beta_c(\infty)$, B, ν and χ^2/d.o.f. are summarized in table 1. The values of $\beta_c(\infty)$ at $N_\tau = 2, 3, 5$ estimated in ref. [19] are systematically smaller than ours beyond the error bars. This may be attributed to the narrow range of N_σ employed in ref. [19]. In table 1 we also list the transition temperature $\beta_c^{X_1}$ and $\beta_c^{X_2}$ determined with the use of the quantities X_1 and X_2 introduced in ref. [4], which show consistency with $\beta_c(\infty)$ within 2 or 3σ error band. Figure 11 shows a typical behavior of the values of X_1 and X_2 as a function of TRG steps. For the values of ν we observe that both of our results and those in ref. [19] are consistent with $\nu = 1$, which is the expected critical exponent in 2D Ising model. This also satisfies the Josephson law of $d\nu = 2 - \alpha$ with $d = 2$ in the two-dimensional case. These are supporting evidences for Svetitsky-Yaffe conjecture that the finite temperature transitions in $(d+1)$-dimensional SU(N) and Z_N lattice gauge theories belong to the same universality class of those in the corresponding d-dimensional Z_N spin models [20]. In our case the universality class for the finite temperature Z_2 lattice gauge theory should coincide with that for the 2D Ising model whose critical exponents are $\alpha = 0$ and $\nu = 1$.

JHEP08(2019)023

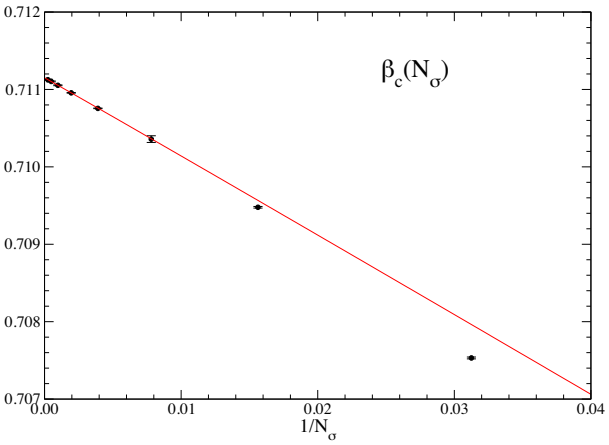

Figure 10. Peak position of the specific heat $\beta_c(N_\sigma)$ at $N_\tau = 3$ as a function of $1/N_\sigma$. Solid curve represents the fit result.

This work							
N_τ	N_σ	$\beta_c(\infty)$	ν	B	χ^2/d.o.f.	$\beta_c^{X_1}$	$\beta_c^{X_2}$
2	$[512, 4096]$	0.656097(1)	1.00(1)	0.116(6)	0.086	0.656094(1)	0.656094(1)
3	$[512, 4096]$	0.711150(4)	0.99(4)	0.10(3)	0.047	0.711151(1)	0.711151(1)
5	$[512, 4096]$	0.740730(3)	0.96(5)	0.08(3)	0.012	0.740734(1)	0.740734(1)
		Ref. [19]					
N_τ	N_σ	$\beta_c(\infty)$	ν				
2	$4, 8, 16, 32$	0.65608(5)	1.012(21)				
3	24	0.71102(8)					
5	40	0.74057(3)					

Table 1. Fit results for the critical point $\beta_c(\infty)$ and the critical exponent ν at $N_\tau = 2, 3, 5$. $\beta_c^{X_1}$ and $\beta_c^{X_2}$ are determined at $N_\sigma \leq 2^{20}$. The value of ν at $N_\tau = 2$ in ref. [19] is evaluated using the pair of data at $N_\sigma = 16$ and 32.

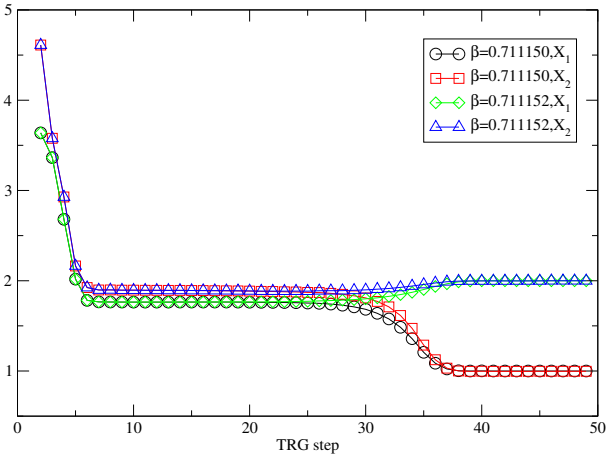

Figure 11. X_1 and X_2 above and below the transition temperature as a function of TRG steps at $N_\tau = 3$.

JHEP08(2019)023

4 Summary and outlook

We have applied the tensor network scheme to a study of 3D finite temperature Z_2 gauge theory. Its efficiency is demonstrated by a numerical study of the critical properties of the 3D Z_2 gauge theory. The tensor network scheme enables us to make a large scale of finite size scaling analysis with the wide range of N_σ thanks to the $\ln V$ dependence of the computational cost, which allows us a precise and reliable estimation of the critical point and the critical exponent at the thermodynamic limit. This is the first successful application of the tensor network scheme to one of the simplest 3D lattice gauge theories. Next step may be the extension of this approach to the gauge theories with continuous groups.

Acknowledgments

Numerical calculation for the present work was carried out with the COMA (PACS-IX) computer under the Interdisciplinary Computational Science Program of Center for Computational Sciences, University of Tsukuba. This work is supported by the Ministry of Education, Culture, Sports, Science and Technology (MEXT) as "Exploratory Challenge on Post-K computer (Frontiers of Basic Science: Challenging the Limits)" and also in part by Grants-in-Aid for Scientific Research from MEXT (No. 15H03651).

References

[1] T. Nishino and K. Okunishi, *Corner transfer matrix renormalization group method*, *J. Phys. Soc. Jpn.* **65** (1996) 891.

[2] N. Maeshima, Y. Hieida, Y. Akutsu, T. Nishino and K. Okunishi, *Vertical density matrix algorithm: a higher dimensional numerical renormalization scheme based on the tensor product state ansatz*, *Phys. Rev.* **E 64** (2001) 016705 [cond-mat/0101360] [INSPIRE].

[3] M. Levin and C.P. Nave, *Tensor renormalization group approach to 2D classical lattice models*, *Phys. Rev. Lett.* **99** (2007) 120601 [cond-mat/0611687] [INSPIRE].

[4] Z.-C. Gu and X.-G. Wen, *Tensor-entanglement-filtering renormalization approach and symmetry protected topological order*, *Phys. Rev.* **B 80** (2009) 155131 [arXiv:0903.1069] [INSPIRE].

[5] Y. Shimizu, *Tensor renormalization group approach to a lattice boson model*, *Mod. Phys. Lett.* **A 27** (2012) 1250035 [INSPIRE].

[6] Y. Shimizu and Y. Kuramashi, *Grassmann tensor renormalization group approach to one-flavor lattice Schwinger model*, *Phys. Rev.* **D 90** (2014) 014508 [arXiv:1403.0642] [INSPIRE].

[7] Z.-C. Gu, F. Verstraete and X.-G. Wen, *Grassmann tensor network states and its renormalization for strongly correlated fermionic and bosonic states*, arXiv:1004.2563 [INSPIRE].

JHEP08(2019)023

[8] Z.-C. Gu, *Efficient simulation of Grassmann tensor product states*, *Phys. Rev.* **B 88** (2013) 115139 [arXiv:1109.4470] [INSPIRE].

[9] Y. Shimizu and Y. Kuramashi, *Critical behavior of the lattice Schwinger model with a topological term at $\theta = \pi$ using the Grassmann tensor renormalization group*, *Phys. Rev.* **D 90** (2014) 074503 [arXiv:1408.0897] [INSPIRE].

[10] Y. Shimizu and Y. Kuramashi, *Berezinskii-Kosterlitz-Thouless transition in lattice Schwinger model with one flavor of Wilson fermion*, *Phys. Rev.* **D 97** (2018) 034502 [arXiv:1712.07808] [INSPIRE].

[11] S. Takeda and Y. Yoshimura, *Grassmann tensor renormalization group for the one-flavor lattice Gross-Neveu model with finite chemical potential*, *Prog. Theor. Exp. Phys.* **2015** (2015) 043B01.

[12] D. Kadoh, Y. Kuramashi, Y. Nakamura, R. Sakai, S. Takeda and Y. Yoshimura, *Tensor network formulation for two-dimensional lattice $N = 1$ Wess-Zumino model*, *JHEP* **03** (2018) 141 [arXiv:1801.04183] [INSPIRE].

[13] R. Sakai, S. Takeda and Y. Yoshimura, *Higher order tensor renormalization group for relativistic fermion systems*, *Prog. Theor. Exp. Phys.* **2017** (2017) 063B07 [arXiv:1705.07764] [INSPIRE].

[14] Y. Yoshimura, Y. Kuramashi, Y. Nakamura, S. Takeda and R. Sakai, *Calculation of fermionic Green functions with Grassmann higher-order tensor renormalization group*, *Phys. Rev.* **D 97** (2018) 054511 [arXiv:1711.08121] [INSPIRE].

[15] Y. Liu et al., *Exact blocking formulas for spin and gauge models*, *Phys. Rev.* **D 88** (2013) 056005 [arXiv:1307.6543] [INSPIRE].

[16] B. Dittrich, F.C. Eckert and M. Martin-Benito, *Coarse graining methods for spin net and spin foam models*, *New J. Phys.* **14** (2012) 035008 [arXiv:1109.4927] [INSPIRE].

[17] B. Dittrich and F.C. Eckert, *Towards computational insights into the large-scale structure of spin foams*, *J. Phys. Conf. Ser.* **360** (2012) 012004 [arXiv:1111.0967] [INSPIRE].

[18] B. Dittrich, S. Mizera and S. Steinhaus, *Decorated tensor network renormalization for lattice gauge theories and spin foam models*, *New J. Phys.* **18** (2016) 053009 [arXiv:1409.2407] [INSPIRE].

[19] M. Caselle and M. Hasenbusch, *Deconfinement transition and dimensional crossover in the 3D gauge Ising model*, *Nucl. Phys.* **B 470** (1996) 435 [hep-lat/9511015] [INSPIRE].

[20] B. Svetitsky and L.G. Yaffe, *Critical behavior at finite temperature confinement transitions*, *Nucl. Phys.* **B 210** (1982) 423 [INSPIRE].

[21] Z.Y. Xie, J. Chen, M.P. Qin, J.W. Zhu, L.P. Yang and T. Xiang, *Coarse-graining renormalization by higher-order singular value decomposition*, *Phys. Rev.* **B 86** (2012) 045139.

JHEP08(2019)023